$[Cu_4OCl_6(DABCO)_2]\cdot 0.5DABCO\cdot 4CH_3OH$ ("**MFU-5**"): Modular synthesis of a zeolite-like metal-organic framework constructed from tetrahedral $\{Cu_4OCl_6\}$ secondary building units and linear organic linkers

Ying-Ya Liu [a], Maciej Grzywa [a], Matthias Weil [b], Dirk Volkmer [a,*]

[a] *Ulm University, Institute of Inorganic Chemistry II-Materials and Catalysis, Albert-Einstein-Allee 11, D-89081 Ulm, Germany*
[b] *Institute for Chemical Technologies and Analytics, Division of Structural Chemistry, Vienna University of Technology, Getreidemarkt 9/164-SC, A-1060 Vienna, Austria*

1. Introduction

The rational design and description of metal-organic framework (MOF) structures rests on the concept of secondary building units (SBUs) which provide suitable geometries and connectivities to erect three-dimensional (3D) coordination frameworks [1–6]. The concept of SBUs was introduced into the field of zeolite structural chemistry, where it is commonly employed to simplify representation of Si–O framework topologies. SBUs of zeolite frameworks are commonly *not* considered as truly existing molecular precursors that precede zeolite formation during synthesis. In the literature relating to MOFs, however, the term SBU often refers to polynuclear coordination units contained in the framework [1,7], which could be clusters [2,8] or metal organic polyhedra [9,10], that have certain coordination environments and sufficiently rigid structures to ensure the "correct" assembly of the network. In this regard, SBUs in MOF synthesis have become useful descriptors as well as supramolecular synthons for a rational design of framework geometries. A large number of MOFs based on particular SBUs (such as the tetranuclear $\{Zn_4O(CO_2)_6\}$ unit acting as octahedral node in the MOF-n series [11–13], the trinuclear $\{Ga_3(PO_4)_3F_2\}$ unit of the MIL-n family [14,15], or the binuclear paddle-wheel $\{Cu_2(CO_2)_4\}$ unit acting as square node in many MOF structures [16–24]) have thus been synthesized through suitable combinations of metal salts and organic linkers [25,26], occasionally employing additional templates [2,3,27–29]. However, apart from a few notable exceptions [9,30–33], MOF topologies reported in literature have *not* resulted from assemblies of rationally designed SBUs. Few studies were focused on studying the particular role of SBUs during MOF formation [34–38]. For example, an EXAFS study has provided experimental evidence that SBUs are present at all stages of crystallization in MOF synthesis [34].

The strategy presented in the current work is to employ SBUs of rationally designed tetranuclear copper precursor complexes (possessing T_d point group symmetry) that become linked into 3D coordination frameworks with suitable organic linkers. Within the framework the local point group symmetry of the original SBUs should be retained. Doing so, we hope to gain better control over MOF design, and to demonstrate the general utility of an

* Corresponding author. Fax: +49 731 50 23039.
E-mail address: dirk.volkmer@uni-ulm.de (D. Volkmer).

SBU-based approach in bottom-up MOF synthesis. In this paper, we present a porous coordination framework built up from $\{Cu_4OCl_6\}$ cluster cores [39,40], connected via DABCO (DABCO = 1,4-diazabicyclo[2.2.2]octane) linkers. A series of tetranuclear complexes of type $[Cu_4OCl_6\mathbf{L}_4]$ (**L** representing monodentate N-, O-, or P-donor ligands) have been reported during the past four decades [39–42]. Owing to the fact that several tens of tetranuclear copper complexes are found in the Cambridge Structural Database [43], the tetrahedral $\{Cu_4OCl_6\}$ coordination unit can be considered as a stable and reliable SBU. It features four coordination sites that can be occupied by monodentate ligands **L**, which are positioned at the corners of a tetrahedron. From a structural point of view, $\{Cu_4OCl_6\}$ cores might be regarded as expanded analogues of *T* atoms, where *T* represents Si, Al or P atoms of TO_4 primary building units in zeolites, which constitute the smallest building units of zeolite-type frameworks. Accordingly, connecting $\{Cu_4OCl_6\}$ cores with rigid linear or bent bidentate organic linkers should then lead to a structure family of novel MOF compounds, which display network topologies similar to known zeolite frameworks. A likewise strategy has been previously realized with so-called zeolitic imidazolate frameworks (ZIFs) [44–49]. A more specific reason for the particular choice of $\{Cu_4OCl_6\}$ SBUs lies in the fact that MOF compounds featuring this unit might display attractive functional properties such as aerobic oxidation catalysis [50,51] or magnetic properties [39,52–54].

As depicted in Scheme 1, within each $\{Cu_4OCl_6\}$ unit four Cu(II) ions are connected through one μ_4-bridging oxide anion resulting in a tetrahedral cluster, in which μ_2-bridging chloride anions are positioned on the edges. Additionally, one monodentate ligand (e.g. MeOH) is coordinated to each Cu(II) ion leading to an overall trigonal-bipyramidal coordination environment of the Cu centres. Ligand exchange of the monodentately bound ligands with bidentate linear ligands such as DABCO then leads to a 3D framework based on tetrahedral $\{Cu_4OCl_6\}$ units. The resulting MOF compound **MFU-5** was characterized by elemental analysis, X-ray diffraction, IR- and UV/Vis spectroscopy. In addition, simultaneous thermal analysis (STA) coupled with mass spectrometry (TG/DTA-MS) was used to elucidate the weight loss stages and the evolution of gaseous products during heat treatment. Details of the single crystal structure as well as the topological analysis of this compound are represented and discussed in the following.

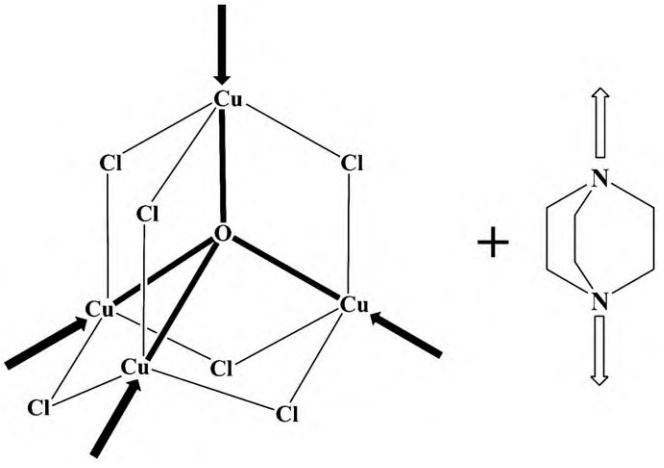

Scheme 1. Schematic representation of the connection principle of 4-connected $\{Cu_4OCl_6\}$ secondary building units (SBUs) and bidentate linear DABCO linkers.

2. Experimental section

2.1. Materials and instruments

All operations were carried out in argon atmosphere. $[Cu_4OCl_6(CH_3OH)_4]\cdot 2CH_3OH$ was prepared according to a published procedure [55]. Methanol was distilled from magnesium before use. All other starting materials were commercially available reagents of analytical grade and used without further purification. Fourier transform infrared (FTIR) spectra were recorded in the region of 400–4000 cm^{-1} in Nujol on a Bruker IFS FTIR spectrometer. Elemental analyses (C, H, N) were carried out on a Perkin-55 Elmer 2400 Elemental Analyzer. Thermogravimetric analysis (TGA) was performed with a TGA/SDTA851 Mettler Toledo analyzer in the temperature range of 25–1100 °C at a heating rate of 10 °C min^{-1} in air flow. Simultaneous thermal analysis (STA) coupled with mass spectrometry (TG/DTA-MS) was employed for investigations on the evolution of gaseous products, which was performed on a NETZSCH STA 409 PC/PG-Luxx thermal analyzer coupled online with a QMS 403C-Aeolos Mass Spectrometer in the temperature range of 25–1100 °C at a heating rate of 5 °C min^{-1} in an atmosphere of flowing argon. Ambient temperature X-ray powder diffraction (XRPD) patterns were measured using a PANalytical X′ Pert PRO diffractometer with X′Celerator detector operated at 40 kV, 40 mA Cu$K\alpha$ radiation (λ = 1.54178 Å) with a scan speed of 30 s $step^{-1}$ and a step size of 0.008°. Variable temperature X-ray powder diffraction (VTXRD) measurements were performed in nitrogen atmosphere with the same diffractometer equipped with an Anton Paar HTK 1200N reaction chamber. Each powder pattern was recorded in the 3–80° range (2θ). From room temperature to 110 °C, the heating rate between recording subsequent patterns was 5 °C/min and once the corresponding temperature was reached, the sample was kept at this temperature for 10 min before starting to measure; from 170 to 200 °C, the heating rate was 1 °C/min, and the sample was held at the corresponding temperature (180, 200 °C) for 5 min; from 300 to 400 °C, the heating rate was readjusted to 5 °C/min again, corresponding to a duration of 10 min before measurement. UV/Vis spectra were recorded with an Analytik Jena Specord UV/Vis spectrometer in the range of 260–1000 nm with a lamp change at 320 nm. The solid samples with poor solubility (**MFU-5**, as well as the oligomeric species (oligomeric species are formed instantaneously after mixing the precursor complex $[Cu_4OCl_6(CH_3OH)_4]\cdot 2CH_3OH$ and DABCO ligands) were ground to a fine powder in an agate mortar, after that the powder was uniformly suspended in methanol solution via ultrasound treatment for 5 min, the homogenous suspension was transferred to a 10 mm path length quartz cuvette where the data was recorded; the DABCO ligand and the precursor complex $[Cu_4OCl_6(CH_3OH)_4]\cdot 2CH_3OH$ were dissolved in methanol, the data were recorded directed from solution; in both cases solvent methanol was used as reference. The concentration of **MFU-5** was $\sim 3\times 10^{-4}$ mol L^{-1} (1 mg suspended in 4 mL methanol), oligomeric species and cluster were at the same concentration based on the copper content. Nitrogen sorption was measured at −196 °C up to 1 bar using a Quantachrome Autosorb-1 apparatus. High purity nitrogen gas (99.999%) was used for the adsorption experiments.

2.2. Solvothermal synthesis of *MFU-5*

0.30 mmol DABCO (33.6 mg) were dissolved in methanol (5 mL), then 0.20 mmol $[Cu_4OCl_6(CH_3OH)_4]\cdot 2CH_3OH$ (135 mg) were added to the solution under vigorous stirring, upon which a dark orange precipitate formed immediately. The suspension was transferred into a 15 mL pyrex tube, sealed, and heated to

110 °C at a rate of 1 °C min^{-1} and kept at this temperature for 24 h. The temperature was then increased to 130 °C, at which the sample was kept for another 2 days. Thereafter, the sample was slowly cooled down to room temperature. In order to remove unreacted precursor complex, the mixture was washed four times with 5 mL portions of acetone. The suspension was subjected to short pulses of ultrasound until the supernatant solution became colorless. Orange crystals (hexagonal columns) were filtered off, washed thoroughly with acetone and dried in air. (Yield: 67%, 84 mg, based on DABCO ligand). C, H, O elemental analysis for $C_{19}H_{46}N_5Cl_6Cu_4O_5$: calcd: C: 25.60; H: 5.20; N: 7.86 (%); found: C: 23.07; H: 4.11; N: 6.85 (%). (Discrepancies between measured and calculated values for elemental composition are most likely due to the presence of Cu ions in the sample). IR: (KBr, cm^{-1}): 3446(br), 2973(w), 2902(w), 2336(w), 1647(m), 1467(s), 1376(w), 1318(m), 1285(w), 1245(w), 1174(w), 1053(s), 1017(m), 925(m), 842(w), 812(s), 649(w), 571(s), 469(w).

2.3. Single crystal X-ray diffraction

Single crystals with a suitable size for structure analysis (at least *ca.* 0.1 mm in length) were selected under a polarizing microscope and fixed on a glass fiber with highly viscous perfluorinated ether (“magic oil”). Reflection intensities of these crystals were pre-checked with Mo$K\alpha$ radiation (0.71073 Å) using a Bruker APEX-II four-circle diffractometer with κ-geometry, equipped with a CCD camera and a Cryostream 600 (Oxford Cryosystems) operating with a stream of nitrogen at −173 °C. The crystal that was finally chosen for the data collection (red-orange colour; columnar-prismatic habit with dimensions of 0.12 × 0.03 × 0.03 mm) had the strongest reflection intensities of all selected crystals and showed sharp diffraction spots up to 20°/θ. Above this angular range the diffraction intensities were too weak to be measured. Thus the complete reciprocal sphere up to this value was recorded with high redundancy, using the *APEX2* [56] program suite for an optimized collection strategy. Data reduction, including corrections for Lorenz and polarization effects, as well as refinement of the lattice parameters were performed with *SAINT* [56]. Intensities were finally corrected for absorption using a multi-scan approach with *SADABS* [56]. The structure was solved by direct methods and refined with the *SHELXL* [57] program package using weighted full-matrix least-squares on F^2. Heavy atoms (Cu and Cl) were initially located from the structure solution; after the first refinement cycles all non-H atoms of the remaining framework atoms were retrieved from the difference Fourier synthesis. The displacement parameters for all non-H atoms were refined anisotropically. Hydrogen atoms were placed in idealized positions and included as riding atoms with a distance constraint of d(C–H) = 0.97 Å. The highest residual electron densities of < 1.4 e$^-$/Å^3 were found in the large channels of **MFU-5**, which we ascribe to the disordered solvent molecules. However, it was not possible to model these molecules sufficiently and therefore we excluded them from refinement. Although the use of PLATON’s SQUEEZE procedure [69] lowered the residuals considerably (R_1 ($I > 2\sigma(I)$ = 0.032, wR_2 (all data) = 0.095), we decided not to use the results based on this correction because the solvent molecules contribute effectively to the stability and to the cohesion of the framework structure.

Selected crystal data and details of structure refinement for **MFU-5** are provided in Table 1. Complete crystallographic data for the structure reported in this paper have been deposited in the CIF format with the Cambridge Crystallographic Data Center as supplementary publication no. CCDC 748777. Copies of the data can be obtained free of charge on application to CCDC, 12 Union Road, Cambridge CB2 1EZ, UK (fax: (44) 1223336-033; e-mail: deposit@ccdc.cam.ac.uk).

Table 1
Crystal data and structure refinement summary for **MFU-5.**

Sample	**MFU-5**
Structured formula	$[Cu_4OCl_6(C_6H_{12}N_2)_2]\cdot 0.5(C_6H_{12}N_2)\cdot 4CH_3OH$
Formula sum	$C_{19}H_{46}N_5Cl_6Cu_4O_5$
M_r	891.50
T (K)	100(2)
Crystal system	Hexagonal
Space group (no)	$P6/mcc$ (192)
a (Å)	25.645(9)
c (Å)	17.105(11)
V (Å^3)	9742(8)
Z	12
D_c (g cm^{-3})	1.823
μ (mm^{-1})	3.116
F(000)	5436
θ Range (°)	2.86–20.44
Refls. total	51791
Refls. unique	1690
Refls. obs.	1302
$R_{int.}/R_{sigma}$	0.1488/0.0344
R_1 ($I>2\sigma(I)$)[a]	0.049
wR_2 (all data)[b]	0.1633
GooF	1.092
Largest diff. peak and hole (Å^{-3})	1.383, −0.517

[a] $R_1 = \sum \|F_0| - |F_c\| / \sum |F_0|$.
[b] $wR_2 = \sum[w(F_0^2 - F_c^2)^2] / \sum[w(F_0^2)^2]^{1/2}$.

3. Results and discussion

3.1. Syntheses and IR characterization

Solvothermal conditions are frequently required in MOF synthesis. Employing microwave irradiation often leads to dramatic rate enhancements and good yields [58–61], as well as good phase selectivity [59,62]. Recent studies have shown that thermodynamically stable products are more favorable for microwave synthesis [59,62], which, however, renders this method less attractive for the synthesis of **MFU-5**. After mixing DABCO linker and the precursor compound in methanol solution, a dark orange colored precipitate forms spontaneously, which we ascribe tentatively to the exchange of MeOH against DABCO ligands at the Cu(II) centres and to rapid formation of oligomeric coordination species. An extended MOF network then forms slowly under solvothermal conditions through continuous ligand exchange and fusion of oligomeric coordination species. Under appropriate reaction conditions the product crystallizes as single phase hexagonal columns, as shown in Fig. 1. Only one crystal habit is observed in SEM micrographs along with optical micrographs, suggesting that no other crystal phases are present in the sample. The phase purity of **MFU-5** was further confirmed by X-ray powder diffraction measurements which are compared to a theoretical diffraction pattern simulated from the diffraction data of the single crystal X-ray structure analysis, as depicted in Fig. 2.

The IR spectrum of **MFU-5** (Fig. S1 in the Supporting Information) shows a strong absorption peak at 571 cm^{-1}, characteristic of the asymmetric vibration (F_2 mode) of the $[Cu_4O]^{6+}$ core [55]. The –OH stretching frequencies in the region of 3446 cm^{-1} and C–O stretching frequency at 1052 cm^{-1}, along with the CH_3 asymmetric deformation vibration at 1467 cm^{-1} can be attributed to free methanol molecules in the crystal lattice.

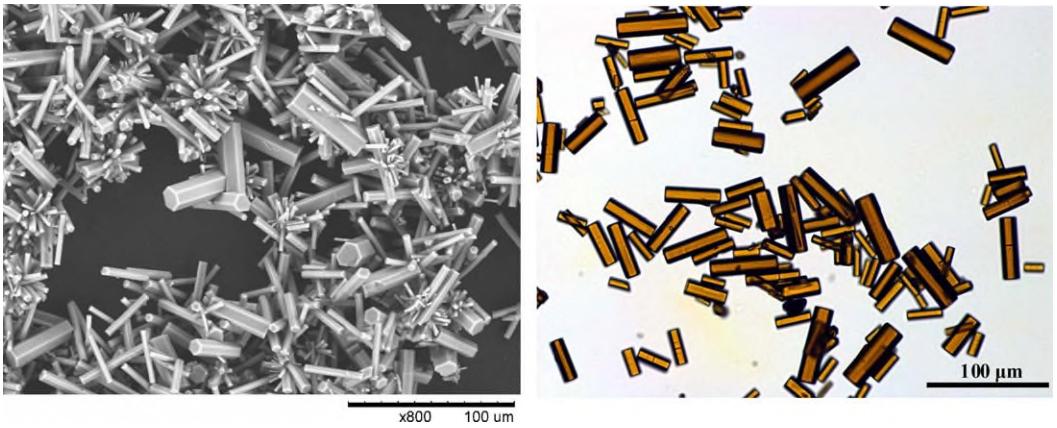

Fig. 1. SEM image (left) and optical micrograph (right) of as-synthesized **MFU-5**.

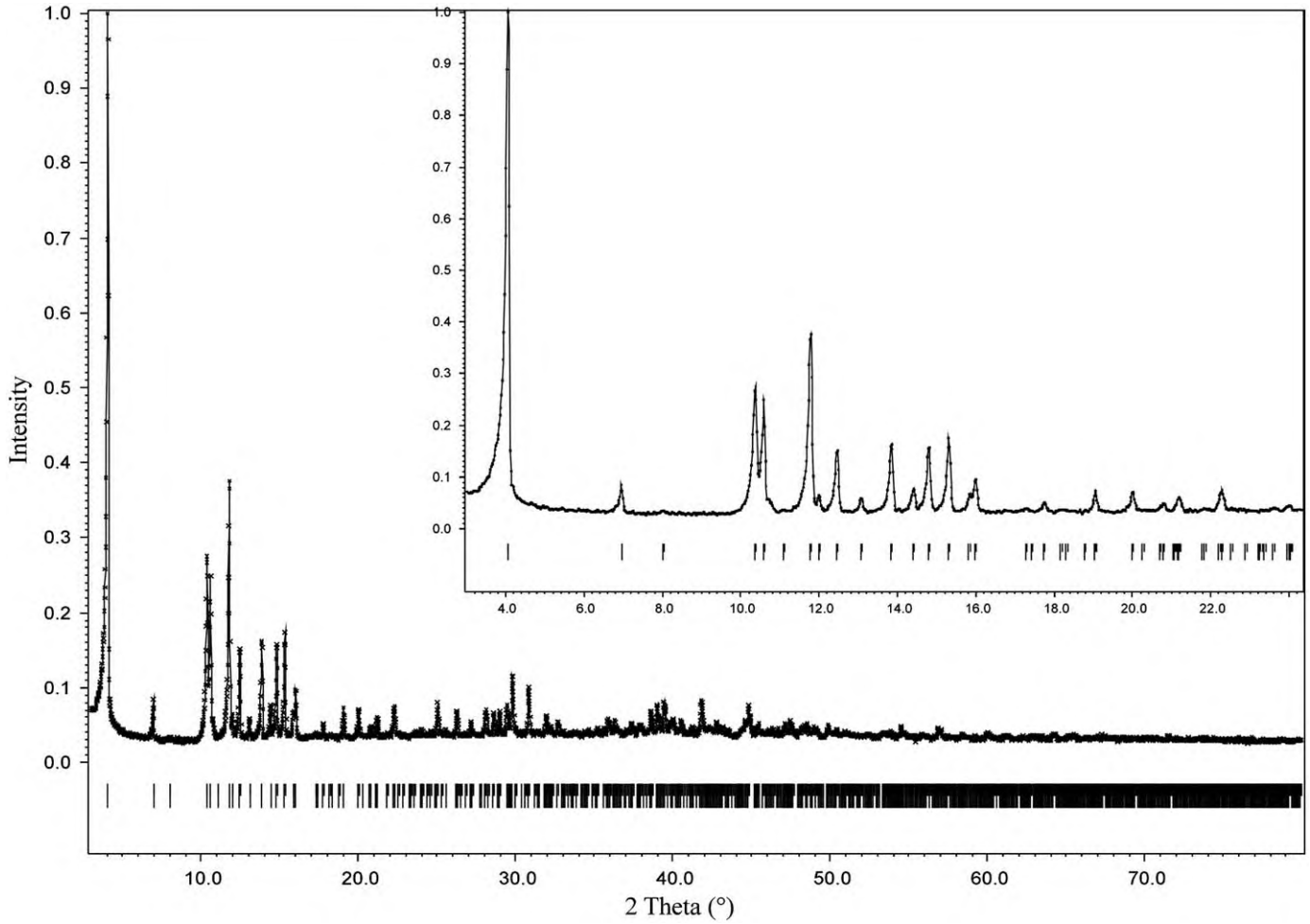

Fig. 2. X-ray powder diffraction pattern of **MFU-5**. The vertical bars correspond to the Bragg peaks calculated from the results of the single crystal structure model. For clarity, the insert shows an expanded view in the range 3–24.5°/2θ.

MFU-5 is stable in most organic solvents such as ethanol, acetonitrile, benzene, toluene, dichloromethane, chloroform and N,N-dimethylformamide. However, the compound decomposes within seconds in pure water in which it transforms into a light blue precipitate, which—according to IR spectroscopy—indicates a complete disassembly of the framework, since the characteristic absorption peak of the $[Cu_4O]^{6+}$ core is not observed any longer (Fig. S2 in the Supporting Information).

3.2. Structure description

An Ortep style plot [63] of the asymmetric unit of **MFU-5** with atom labels is shown in Fig. 3. This unit consists of three copper atoms, one oxygen, four chlorine, seven carbon and three nitrogen atoms. The atomic coordinates and isotropic temperature factors, selected bond lengths and angles for **MFU-5** are presented in Tables S1 and S2 in the Supporting Information.

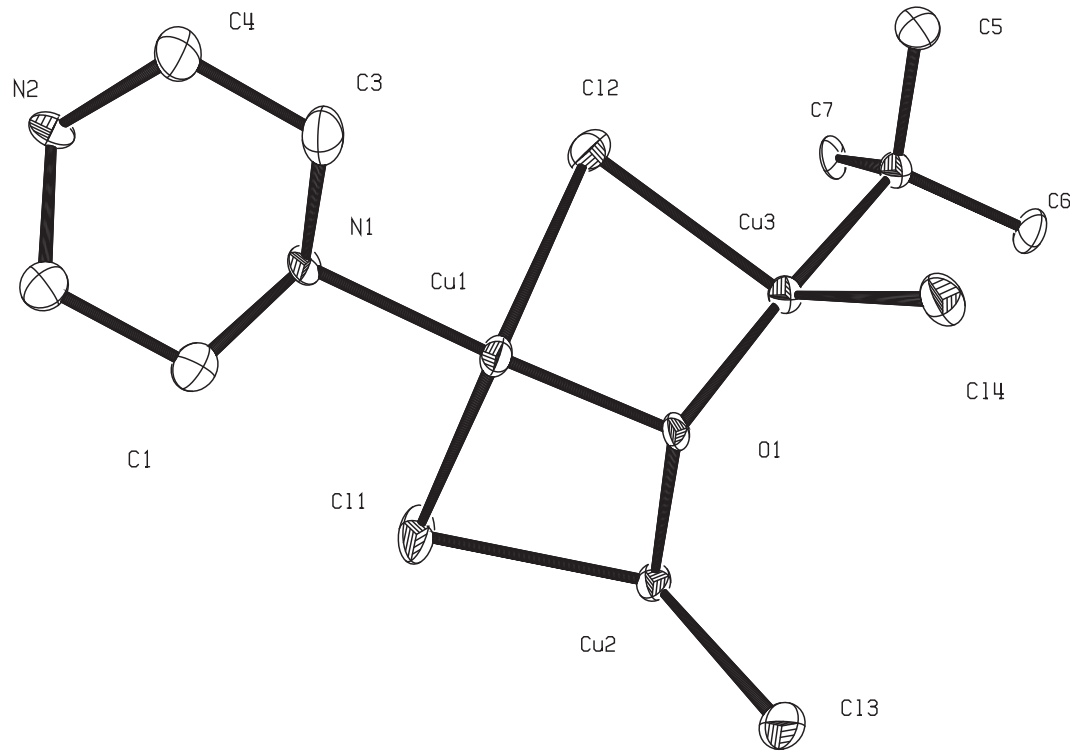

Fig. 3. View of the asymmetric unit of **MFU-5** showing the atom numbering scheme. Displacement ellipsoids are drawn at the 50% probability level; hydrogen atoms are omitted for clarity.

3.2.1. *Structure of the {Cu_4OCl_6} building unit in* ***MFU-5***

As depicted in Fig. 4, the copper(II) centres in the {Cu_4OCl_6} building unit of **MFU-5**, are positioned tetrahedrally around a central oxide anion. Pairs of copper ions are bridged by chloride ligands, which are aligned centrally on the edges of an imaginary Cu tetrahedron. The interatomic distances and bond angles are close to those reported for low molecular weight [$Cu_4OCl_6\mathbf{L}_4$] complexes [40,41,52]. The six chloride ions surrounding the tetrahedral {Cu_4O} coordination unit form a slightly distorted octahedron.

3.2.2. *Structure of* ***MFU-5***

MFU-5 adopts a new structure type and crystallizes in the hexagonal crystal system in space group *P*6/*mcc* (no. 192). The {Cu_4OCl_6} core serves as four-connected node which is cross-linked via bidentate DABCO ligands into a three-dimensional (3D) network (Fig. 4a, b). In the [$Cu_4OCl_6(DABCO)_2$] framework, Cu–N bond distances range from 1.979(12) to 2.000(9) Å. It is noteworthy that the N–O–N angles range from 107.0 to 110.4°, which is very close to the values of the TO_4 primary building unit (T_1 unit) in zeolites with a mean value of 109.8°. A structural analogy can thus be drawn between T_1 units of zeolite frameworks and **MFU-5**, according to which the {Cu_4OCl_6} coordination unit can be treated as *T* unit and DABCO takes the places of O^{2-} ions. Thus, the tetrahedral unit {$Cu_4OCl_6N_4$} (referred to as a T_1 unit hereafter, in which "N" represent the coordinated nitrogen atom of the DABCO ligand) in the **MFU-5** framework can be simplified as shown in Fig. 4c, which displays a zeolite-like structure. The grey and black colors, respectively, represent two structurally independent nets existing in the framework. Referring to Fig. 4b for comparison (the highlighted orange and blue colors also show two interpenetrated nets, which will be discussed later), six adjacent T_1 units are connected to each other to form a six-membered ring, which is parallel to the *ab* plane of the crystal lattice.

As shown in Fig. 4e, larger coordination cages comprising 18 T_1 units altogether are formed *via* cross-linking hexagonal T_6 rings, which will be subsequently referred to as a {6^8} cage, as depicted in Fig. 4d. A closer inspection reveals that the {6^8} cage has an inner height of 14.1 Å, the aperture of the large hexagonal pore is between 9.4 and 11.4 Å, and the internal diameter is about 23.8 Å (neglecting van der Waals radii). According to the International Zeolite Association (IZA) this {6^8} cage is a composite building unit of zeolitic networks, namely *mso* [64], which contains 18 *T* atoms. It is the basic unit found in a number of structurally different zeolite framework of the type **SSF** [65], **MSO** [66] and **SZR** [64,67]. However, the connectivity of *mso* cages in **MFU-5** should be distinguished from those in **SSF**, **MSO** and **SZR**. These zeolite frameworks generally contain further composite building units to interconnect *mso* cages, while the **MFU-5** framework is constructed by the fusion of *mso* cages only, as shown in Fig. S3. Therefore, **MFU-5** displays a novel structure that cannot be categorized within the current zeolite framework types. Among the zeolite compounds cited above, the *mso* cage has a height of about 3.1 Å, the aperture of the hexagonal window is about 2.2 × 2.2 Å, and the internal diameter is about 4.1 Å. In contrast to zeolite networks, coordination frameworks might become interpenetrated quite easily [68]. In **MFU-5**, the connection of T_1 units produces a 3D network which is spacious enough to host a second, structurally identical network, as depicted schematically in Fig. 4d and e (topologically independent networks are distinguished by colors). Each network is generated by fusing *mso* cages into columns running along the *c*-axis. These columns then become fused into networks by sharing column walls. Two independent networks interpenetrate each other in a staggered fashion. It is worth noting that despite of interpenetration, **MFU-5** still maintains 1D channels with a large inner diameter of approximately 11.4 Å (measured between centers of two opposite chlorine atoms, neglecting van der Waals radii). These channels

are densely packed with methanol and non-coordinated DABCO molecules as revealed by elemental and thermogravimetric analysis. However, owing to structural disorder no guest molecules could be located in the channels of **MFU-5** during structure analysis from X-ray diffraction data. Based on calculations performed with PLATON [69], **MFU-5** has a void volume of 36.9% per unit cell volume (3597.8 Å^3 per 9742(8) Å^3) if the occluded molecules were omitted. Based on an average atom volume method [70], the calculated average volume (at 25 °C) of a single methanol molecule and of a DABCO molecule, respectively, amounts to 46 and 169 Å^3. Based on this estimate, there should be sufficient space for approximately 4.6 methanol and 0.5 DABCO molecules per **MFU-5** unit cell, to become occluded within the channels of the framework. Results from thermogravimetric analysis are in good agreement with this estimation and confirm the presence of additional 4 methanol molecules and 0.5 DABCO molecules per formula unit. Moreover, the total amount of 2.5 DABCO molecules per formula unit (i.e. 2 coordinated and 0.5 occluded molecules) in **MFU-5** is confirmed by dissolution of the as-synthesized material and subsequent analysis of the organic residue (a detailed description is given in the Supporting Information).

MFU-5 shows a zeolite-like structure due to the presence of $\{Cu_4OCl_6N_4\}$ T_1 units. Based on the rigid and stable $\{Cu_4OCl_6\}$ SBU, we might be able to construct novel zeolite-like frameworks by replacing the bidentate linear DABCO linker with multidentate linkers or bidentate linkers possessing bite angles deviating from 180°. Changing linear DABCO linkers into bent counterparts could offer more possibilities to build up different zeolite-type framework. Combining pyrimidine derivatives with tetrahedral $\{Cu_4OCl_6\}$ nodes, for instance, might lead to *sod*-type zeolites [71], whereas imidazolate units could form 145° angles between adjacent $\{Cu_4OCl_6\}$ cores, which coincides with typical Si–O–Si angles in zeolites. (Si–O–Si angles in zeolites are flexible enough to cover a wide range from 140 up to 165°, however, angle values of approximately 147° are found in many structures [72]). This

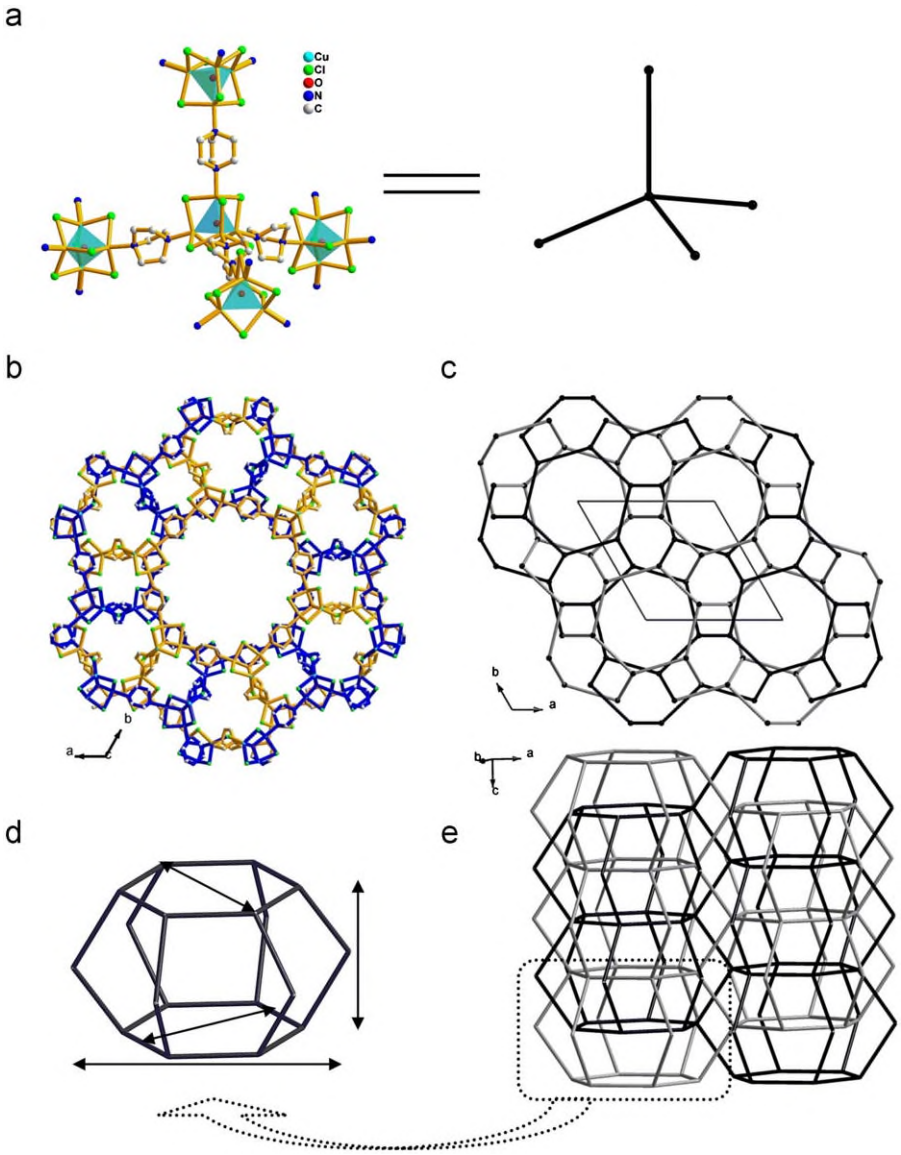

Fig. 4. (a) Left: Ball-and-stick model of a T_1 unit in **MFU-5** connected via DABCO linkers to four adjacent T_1 units. Right: simplified wire representation of the same units (right). (b) Packing diagram of **MFU-5** projected along the *c*-axis, the blue and orange colors distinguish two independent interpenetrated nets; (c) Same packing diagram of **MFU-5** presented as wire model. (d) Periodic building unit of **MFU-5**: *mso* cage; (e) Wire Model of **MFU-5** highlighting the fusion of *mso*-type cages into channels and the concomitant two-fold interpenetration of networks. (For interpretation of the references to color in this figure legend, the reader is referred to the web version of this article.)

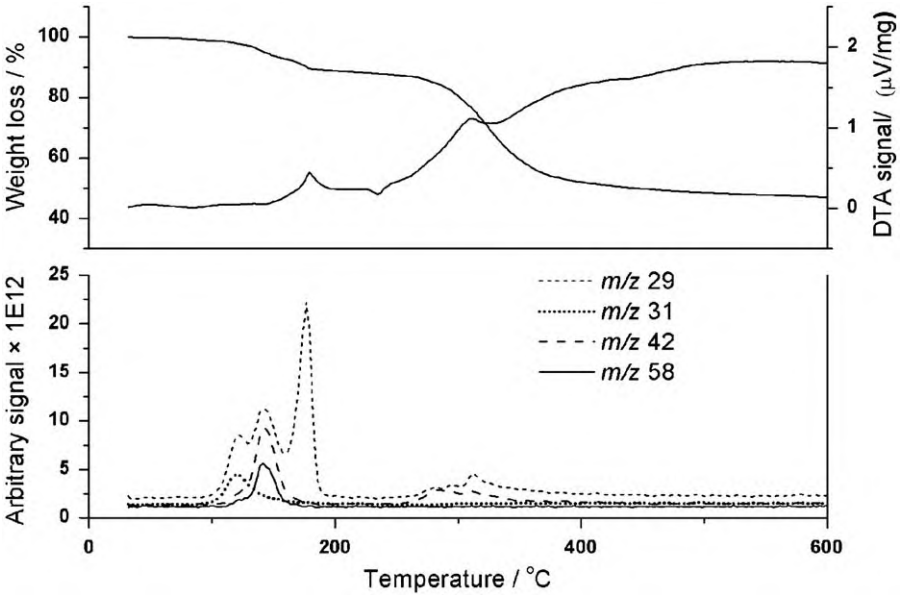

Fig. 5. (top) TG, DTA traces from 20 to 600 °C for a sample kept under argon atmosphere. The traces underneath show temperature profiles of selected fragments of **MFU-5** during the thermogravimetric experiment.

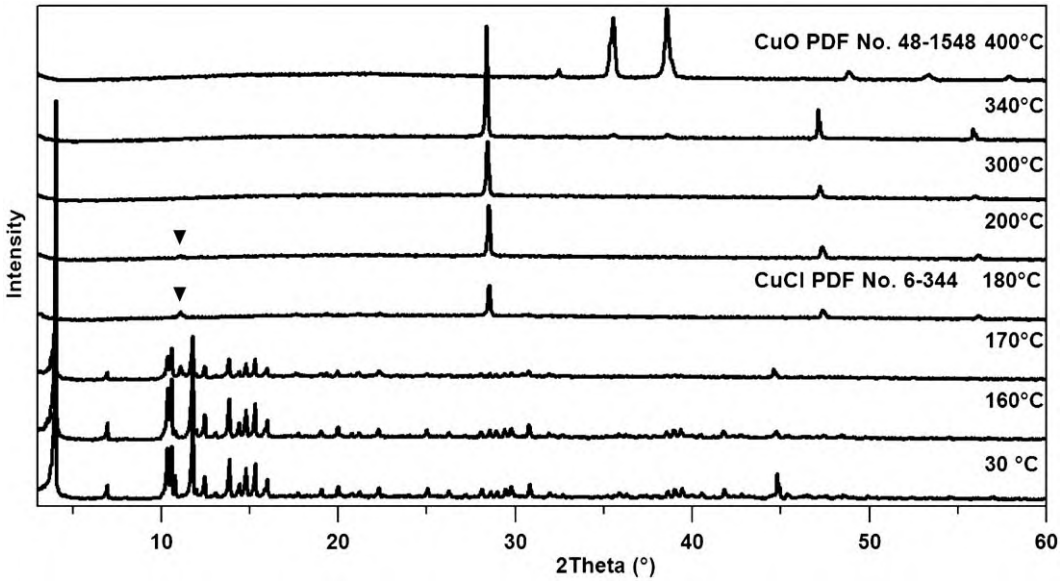

Fig. 6. Powder X-ray diffraction patterns of **MFU-5** in the temperature range 30 to 400 °C. Reflections marked with a solid triangle belong to unidentified phase(s).

type of building block approach has been demonstrated successfully in the construction and synthesis of zeolitic imidazolate frameworks [44–46,49].

3.3. Thermal behavior

By heating **MFU-5** under argon atmosphere, many types of pertinent cleavage reactions are observed in the mass spectrum. As shown in Fig. 5, the TG/DTA-MS results show two exothermic reactions in the DTA measurement, which are accompanied with a total mass loss of 53% before 600 °C in the TG experiment. The detection of a CH_3O fragment was observed with the maximum fragment count being encountered at 122 °C; at about the same temperature, a CHO fragment was also detected. The two fragments stem from weakly bound methanol molecules which are presumably held by weak forces (hydrogen bonds and van der Waals interactions) within the channels of the main framework. At 142 °C, C_2H_4N and $C_2H_6N_2$ fragments were observed, accompanied by peaks with m/z=29 and with m/z=85 that originate from a $C_4H_9N_2$ fragment. Any of these fragments originate from piperazine, $C_4H_{10}N_2$. Since ^{1}H-NMR studies (Fig. S4 in the Supporting Information) indicate unequivocally that DABCO is the only N-containing organic component of **MFU-5** (detailed description are given in the Supporting Information), piperazine is formed by decomposition of DABCO molecules under conditions of the thermogravimetric experiment. It is known from literature that free DABCO molecules (melting point: 155–160 °C, sublimation temperature under atmospheric pressure: 140 °C) is thermally unstable, with decomposition starting from 86 °C and decomposition products being either piperazine or 4, 4′-ethylenedipiperazine [73–76]. However, DABCO ligands that are coordinated to metal ions exhibit

a delayed decomposition process, as shown by the decomposition temperatures of M(DABCO)Cl_2 (M=Cu, Ni, Co, Fe, Mn) complexes that range from 101 to 206 °C [76].

The thermal stability of $[Cu_4OCl_6\mathbf{L}_4]$ compounds depends strongly on the bonding properties of neutral ligands [42]. As shown in Fig. 6, VT-XRPD analysis shows the **MFU-5** framework to be stable up to 160 °C. Small changes in the diffraction pattern are observed at 170 °C. Although the diffraction pattern at 170 °C is similar to those obtained at lower temperatures, the reflection intensities become weaker, especially with increasing 2θ values; the Bragg reflection at 10.79° has disappeared, while new reflections at 11.08, 19.36, 30.43° are recorded; the strong reflection at 11.08° is observed up to 200 °C. Two major structural changes occur at 180 and 400 °C, respectively. The overall changes of X-ray diffraction properties are in agreement with TGA results (Fig. 7). The TG curve recorded under dynamic air atmosphere displays a well-developed plateau, which reveals an initial weight loss (obsd: 7.2%) below 70 °C that can be assigned to the release of weakly bound methanol molecules trapped within the channels. This percentage corresponds to an amount of approximately 4 methanol molecules per formula unit (calcd: 7.2%). A second major weight loss (obsd: 6.7%) occurs between 130 and 205 °C, which is attributed to the decomposition and release of 0.5 free DABCO molecules per formula unit (calcd: 6.3%). Since there is no obvious plateau in the TG curve, a gradual collapse of the framework structure occurs upon release of free DABCO molecules. Coincidently, VT-XRPD shows that from 180 to 340 °C, the phase CuCl (PDF File No. 6–344) forms as a major decomposition product, with one additional unidentified peak at 11.08° that represents the formation of an as-yet unassigned phase. Previous reports in fact have demonstrated that Cu(II) can be reduced to Cu(I) by *N*-donor ligands [42,77]. At 400 °C, the formation of CuO (PDF File No. 48-1548) is observed from VT-XRPD, which was also identified as the final residue from the TGA experiment (obsd: 24.3%, calcd: 35.7%). It should be noted that the observed overall weight loss of **MFU-5** is considerably higher than the theoretical value. We assume that this is caused by premature sublimation of Cu(II) as a volatile Cl-containing complex, as reported in previous studies [42]. There are also some differences in temperature dependent structural changes if the results from TGA and VT-XRPD are compared directly with each other. This might be attributed to the difference in heating procedures since for both experiments different heating rates and conditions were employed, e.g. the samples are kept at a constant temperature for several minutes during VT-XRPD experiments, whereas the samples are subjected to a constantly increasing temperature during TGA experiments.

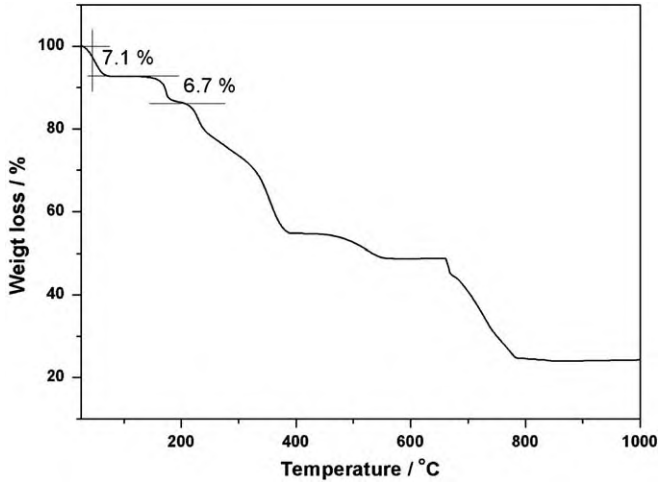

Fig. 7. TG curve of a sample of **MFU-5** kept in flowing air.

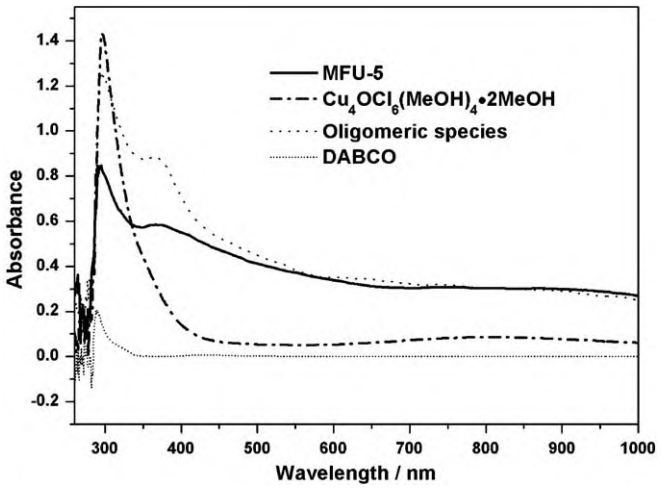

Fig. 8. UV/Vis absorption spectra of **MFU-5**, precursor complex $[Cu_4OCl_6(CH_3OH)_4]\cdot 2CH_3OH$, DABCO ligand, and oligomeric species formed instantaneously after mixing the precursor complex $[Cu_4OCl_6(CH_3OH)_4]\cdot 2CH_3OH$ and DABCO ligands.

3.4. UV/vis spectra

The UV/Vis spectra of **MFU-5**, the precursor complex $[Cu_4OCl_6(CH_3OH)_4]\cdot 2CH_3OH$ and of free DABCO ligands in methanol solution are displayed in Fig. 8. For better comparison, the UV/Vis data of oligomeric species which are formed instantly after mixing the precursor complex and DABCO linker, are also included. The DABCO ligand shows no absorption bands in the UV/vis spectrum. **MFU-5**, oligomeric species and the $[Cu_4OCl_6(CH_3OH)_4]\cdot 2CH_3OH$ precursor display a similar absorption peak with the maximum centered at 296 nm in the UV region. Both **MFU-5** and the oligomeric species show another weak absorption peak with a maximum centered at 370 nm, which could be assigned to the LMCT (ligand to metal charge transfer) occurring between the DABCO ligand and copper(II) centers [78,79].

3.5. N_2 sorption measurements

Major efforts were focused on the appropriate pre-treatment of **MFU-5** samples in order to release occluded molecules without leading to framework collapse. Two pre-treatment methods (exchange with chloroform [80] and exchange with supercritical carbon dioxide [81]) were carried out (see detailed procedures in Supporting Information). However, both strategies were found to be unsuitable for the purpose to remove occluded molecules completely, as depicted in Fig. S5. Further attempts to remove occluded molecules by heating the sample in vacuum to 110 and 130 °C, respectively, invariably resulted in the collapse of the pore system, as shown in Fig. S6. Compared to the XRPD pattern of as-synthesized **MFU-5,** sample treatment at 130 °C under reduced pressure leads to a complete new crystal phase due to the release of the bound methanol molecules, which was not observed during VT-XRPD measurements of as-synthesized **MFU-5**. Heating the sample up to 110 °C under reduced pressure reveals a XRPD pattern with the main reflections getting weaker and new diffraction peaks appearing if compared with the as-synthesized **MFU-5.** These experiments indicate strongly that solvent removal is accompanied with structural changes, i.e. collapse of the **MFU-5** framework structure. This assumption gains further support from

N_2 sorption measurements conducted at −196 °C: after complete removal of occluded methanol molecules (by performing a supercritical CO_2 exchange and keeping the sample overnight under vacuum at 50 °C) **MFU-5** shows a very low surface area (S_{BET}=78 m^2/g, $S_{Langmuir}$=118 m^2/g). Raising the temperature to 110 and 130 °C, respectively, finally leads to an essentially non-porous material, as indicated by a N_2 sorption experiments that reveal a vanishing surface area. It should be pointed out here that the N_2 sorption isotherm (Fig. S7) of the samples do not show the trace of adsorption isotherms typical of microporous solids which is attributed to a continuous decomposition of the samples during the measurement.

4. Conclusions

The work reported here focuses on the modular synthesis of open metal-organic frameworks based on the $\{Cu_4OCl_6\}$ cluster core. With the strategy of a SBU-based bottom-up MOF synthesis, we have successfully synthesized a zeolite-like MOF $[Cu_4OCl_6(DABCO)_2]\cdot 0.5DABCO\cdot 4CH_3OH$ (**MFU-5**) constructed from the $\{Cu_4OCl_6\}$ SBU and linear DABCO linkers. The tetrahedral $\{Cu_4OCl_6N_4\}$ unit can be regarded as an expanded analogue of T_1 units that are present in zeolite structures. The utility of this rational approach lies in the fact that novel zeolite-type MOFs might be developed rapidly by replacing the DABCO ligands with other types of bi- or multidentate linkers. **MFU-5** can be described as a two-fold interpenetrated 3D framework, built up by fusing *mso*-type cages. The interpenetrated structure still maintains 1D channels with a large inner diameter of 11.4 Å. Disordered methanol and DABCO molecules are located in the channels. Removing occluded molecules from **MFU-5** by heating leads to a non-porous material. The UV/vis spectrum shows a LMCT absorption band at λ_{max}=370 nm. Considering the catalytic performance of $\{Cu_4OCl_6\}$ cluster and Cu(II)-based catalyst in aerobic oxidation reactions [50,82,83], we expect **MFU-5** and structurally related zeolite-type MOFs to feature potential applications in catalytic reactions, presumably under mild conditions. However, the stability of the novel compound **MFU-5** presented here as yet is insufficient for catalytic reactions being combined with size-exclusion effects, since a partial to complete framework collapse occurs upon removal of occluded solvent molecules and thus a permanent porosity cannot be retained. Work on MOF structures based on $\{Cu_4OCl_6\}$ SBUs which show an enhanced framework stability are currently being performed in our laboratories.

Supporting information

Supporting information containing IR analysis of **MFU-5**, the crystallographic information file (CIF) for **MFU-5**, a detailed description of acidic treatment of **MFU-5** and pre-treatment of samples prior to N_2 sorption measurement as well as a comparison of the corresponding TG and XRPD measurements of the samples, is available on the Web under http://www.sciencedirect.com or from the authors.

Acknowledgments

Financial Support by the DFG (Priority Program SPP 1362 "Porous Metal-organic Frameworks") is gratefully acknowledged. The authors acknowledge Dr. Irena Senkovska (Department of Inorganic Chemistry, Dresden University of Technology) for help with TG/DTA-MS measurements and Markus Tonigold (Institute of Inorganic Chemistry II, Ulm University) for help with gas sorption measurements.

Appendix A. Supplementary material

Supplementary data associated with this article can be found in the online version at doi:10.1016/j.jssc.2009.10.026.

References

[1] M. Eddaoudi, D.B. Moler, H. Li, B. Chen, T.M. Reineke, M. O'Keeffe, O.M. Yaghi, Acc. Chem. Res. 34 (2001) 319.
[2] Q.R. Fang, G.S. Zhu, Z. Jin, M. Xue, X. Wei, D.J. Wang, S.L. Qiu, Angew. Chem. Int. Ed. 45 (2006) 6126.
[3] J. Kim, B. Chen, T.M. Reineke, H. Li, M. Eddaoudi, D.B. Moler, M. O'Keeffe, O.M. Yaghi, J. Am. Chem. Soc. 123 (2001) 8239.
[4] N.L. Rosi, M. Eddaoudi, J. Kim, M. O'Keeffe, O.M. Yaghi, Angew. Chem. Int. Ed. 41 (2002) 284.
[5] N.L. Rosi, J. Kim, M. Eddaoudi, B. Chen, M. O'Keeffe, O.M. Yaghi, J. Am. Chem. Soc. 127 (2005) 1504.
[6] O.M. Yaghi, M. O'Keeffe, N.W. Ockwig, H.K. Chae, M. Eddaoudi, J. Kim, Nature 423 (2003) 705.
[7] N.W. Ockwig, O. Delgado-Friedrichs, M. O'Keeffe, O.M. Yaghi, Acc. Chem. Res. 38 (2005) 176.
[8] J.R. Li, Y. Tao, Q. Yu, X.H. Bu, Chem. Commun. (2007) 1527.
[9] Y. Zou, M. Park, S. Hong, M.S. Lah, Chem. Commun. (2008) 2340.
[10] J.J. Perry IV, J.A. Perman, M.J. Zaworotko, Chem. Soc. Rev. 38 (2009) 1400.
[11] M. Eddaoudi, J. Kim, N. Rosi, D. Vodak, J. Wachter, M. O'Keefe, O.M. Yaghi, Science 295 (2002) 469.
[12] H.K. Chae, J. Kim, O.D. Friedrichs, M. O'Keefe, O.M. Yaghi, Angew. Chem. Int. Ed. 42 (2003) 3907.
[13] H. Chun, H. Jung, Inorg. Chem. 48 (2009) 417.
[14] C. Sassoye, J. Marrot, T. Loiseau, G. Férey, Chem. Mater. 14 (2002) 1340.
[15] L. Beitone, J. Marrot, T. Loiseau, G. Férey, M. Henry, C. Huguenard, A. Gansmuller, F. Taulelle, J. Am. Chem. Soc. 125 (2003) 1912.
[16] M. Eddaoudi, J. Kim, M. O'Keeffe, O.M. Yaghi, J. Am. Chem. Soc. 124 (2002) 376.
[17] N. Mercier, A. Riou, Chem. Commun. 10 (2004) 844.
[18] Z. Ni, A. Yassar, T. Antoun, O.M. Yaghi, J. Am. Chem. Soc. 127 (2005) 12752.
[19] L. Wang, M. Yang, Z. Shi, Y. Chen, S. Feng, J. Solid State Chem. 178 (2005) 3359.
[20] H. Furukawa, J. Kim, K.E. Plass, O.M. Yaghi, J. Am. Chem. Soc. 128 (2006) 8398.
[21] H. Kumagai, M. Akita-Tanaka, K. Inoue, K. Takahashi, H. Kobayashi, S. Vilminot, M. Kurmoo, Inorg. Chem. 46 (2007) 5949.
[22] M. Du, R.Q. Zou, R.Q. Zhong, T. Yamada, G. Maruta, S. Takeda, Q. Xu, Inorg. Chim. Acta 361 (2008) 1827.
[23] M. Xue, G. Zhu, Y. Li, X. Zhao, Z. Jin, E. Kang, S. Qiu, Cryst. Growth Des. 8 (2008) 2478.
[24] M.J. Prakash, Y. Zou, S. Hong, M. Park, M.-P.N. Bui, G.H. Seong, M.S. Lah, Inorg. Chem. 48 (2009) 1281.
[25] G. Férey, C. Mellot-Draznieks, C. Serre, F. Millange, J. Dutour, S. Surble, I. Margiolaki, Science 309 (2005) 2040.
[26] G. Férey, C. Serre, C. Mellot-Draznieks, F. Millange, S. Surble, J. Dutour, I. Margiolaki, Angew. Chem. Int. Ed. 43 (2004) 6296.
[27] G. Férey, J. Solid State Chem. 152 (2000) 37.
[28] M. Eddaoudi, J. Kim, N. Rosi, D. Vodak, J. Wachter, M. O'Keeffe, O.M. Yaghi, Science 295 (2002) 469.
[29] J.J. Zhang, Y. Zhao, S.A. Gamboa, M. Muñoz, A. Lachgar, Eur. J. Inorg. Chem. (2008) 2982.
[30] J.P. Lang, Q.F. Xu, R.X. Yuan, B.F. Abrahams, Angew. Chem. Int. Ed. 43 (2004) 4741.
[31] J. Zhang, A. Lachgar, J. Am. Chem. Soc. 129 (2007) 250.
[32] J. Park, S. Hong, D. Moon, M. Park, K. Lee, S. Kang, Y. Zou, R.P. John, H.K. Ghyung, S.L. Myoung, Inorg. Chem. 46 (2007) 10208.
[33] Y.L. Bai, J. Tao, R.B. Huang, L.S. Zheng, Angew. Chem. Int. Ed. 47 (2008) 5344.
[34] S. Surblé, F. Millange, C. Serre, G. Férey, R.I. Walton, Chem. Commun. (2006) 1518.
[35] O. Shekhah, H. Wang, S. Kowarik, F. Schreiber, M. Paulus, M. Tolan, C. Sternemann, F. Evers, D. Zacher, R.A. Fischer, C. Wöll, J. Am. Chem. Soc. 129 (2007) 15118.
[36] S. Hermes, T. Witte, T. Hikov, D. Zacher, S. Bahnmüller, G. Langstein, K. Huber, R.A. Fischer, J. Am. Chem. Soc. 129 (2007) 5324.
[37] M. Shoaee, M.W. Anderson, M.P. Attfield, Angew. Chem. Int. Ed. 47 (2008) 8525.
[38] R.E. Morris, Chem. Phys. Chem. 10 (2009) 327.
[39] A.M. Atria, A. Vega, M. Contreras, J. Valenzuela, E. Spodine, Inorg. Chem. 38 (1999) 5681.
[40] J.A. Bertrand, J.A. Kelley, J. Am. Chem. Soc. 88 (1966) 4746.
[41] P. Cortes, A.M. Atria, M.T. Garland, R. Baggio, Acta Crystallogr. Sect. C Cryst. Struct. Commun. 62 (2006) M311.

[42] H. Langfelderová, D. Makáová, V. Jorík, J. Therm. Anal. 41 (1994) 37.
[43] Cambridge Structural Database, Cambridge Crystallographic Data Centre, 〈www.ccdc.cam.ac.uk〉.
[44] Y.Q. Tian, C.X. Cai, Y. Ji, X.Z. You, S.M. Peng, G.H. Lee, Angew. Chem. Int. Ed. 41 (2002) 1384.
[45] Y.Q. Tian, C.X. Cai, X.M. Ren, C.Y. Duan, Y. Xu, S. Gao, X.Z. You, Chem. Eur. J. 9 (2003) 5673.
[46] H. Hayashi, A.P. Côté, H. Furukawa, M. O'Keeffe, O.M. Yaghi, Nat. Mater. 6 (2007) 501.
[47] Y.Q. Tian, Y.M. Zhao, Z.X. Chen, G.N. Zhang, L.H. Weng, D.Y. Zhao, Chem. Eur. J. 13 (2007) 4146.
[48] R. Banerjee, A. Phan, B. Wang, C. Knobler, H. Furukawa, M. O'Keeffe, O.M. Yaghi, Science 319 (2008) 939.
[49] B. Wang, A.P. Côté, H. Furukawa, M. O'Keeffe, O.M. Yaghi, Nature 453 (2008) 207.
[50] H. Sun, K. Harms, J. Sundermeyer, J. Am. Chem. Soc. 126 (2004) 9550.
[51] M.R. Churchill, F.J. Rotella, Inorg. Chem. 18 (1979) 853.
[52] R. Boca, L. Dlhan, D. Makanova, J. Mrozinski, G. Ondrejovic, M. Tatarko, Chem. Phys. Lett. 344 (2001) 305.
[53] P. Cortes, A.M. Atria, M. Contreras, M.T. Garland, O. Pena, G. Corsini, J. Chil. Chem. Soc. 51 (2006) 957.
[54] R.C. Dickinson, W.A. Baker, T.D. Black, R.S. Rubins, J. Chem. Phys. 79 (1983) 2609.
[55] H. Tom Dieck, H.-P. Brehm, Chem. Ber. 102 (1969) 3577.
[56] APEX2, SADABS and SAINT. Bruker Analytical X-ray Instruments Inc., Madison, Wisconsin, USA.
[57] G. Sheldrick, Acta Cryst. A 64 (2008) 112.
[58] S.H. Jhung, J.S. Chang, J.S. Hwang, S.E. Park, Micropor. Mesopor. Mater. 64 (2003) 33.
[59] S.H. Jhung, J.H. Lee, P.M. Forster, G. Férey, A.K. Cheetham, J.S. Chang, Chem. Eur. J. 12 (2006) 7899.
[60] S. Biswas, M. Tonigold, D. Volkmer, Z. Anorg. Allg. Chem. 634 (2008) 2532.
[61] Y. Lu, M. Tonigold, B. Bredenkötter, D. Volkmer, J. Hitzbleck, G. Langstein, Z. Anorg. Allg. Chem. 634 (2008) 2411.
[62] S.H. Jhung, T. Jin, J.S. Hwang, J.S. Chang, J. Nanosci. Nanotechnol. 7 (2007) 2734.
[63] L.J. Farrugia, Ortep-3 for Windows, J. Appl. Cryst. 30 (1997) 565.
[64] Ch. Baerlocher, L.B. McCusker, Database of Zeolite Structures: 〈http://www.iza-structure.org/databases/〉.
[65] S. Elomari, A.W. Burton, K. Ong, A.R. Pradhan, I.Y. Chan, Chem. Mater. 19 (2007) 5485.
[66] D.F. Shantz, A. Burton, R.F. Lobo, Micropor. Mesopor. Mater. 31 (1999) 61.
[67] S.L. Lawton, J.M. Bennett, J.L. Schlenker, M.K. Rubin, Chem. Commun. (1993) 894.
[68] S.R. Batten, R. Robson, Angew. Chem. Int. Ed. 37 (1998) 1461.
[69] A.L. Spek, Acta Cryst. D 65 (2009) 148.
[70] D.W.M. Hofmann, Acta Cryst. B 58 (2002) 489.
[71] L.C. Tabares, J.A.R. Navarro, J.M. Salas, J. Am. Chem. Soc. 123 (2001) 383.
[72] R.F. Lobo, Handbook of Zeolite Science and Technology, Marcel Dekker Inc, 2003.
[73] K.E. Knope, C.L. Cahill, Inorg. Chem. 46 (2007) 6607.
[74] M. Dan, J.N. Behera, C.N.R. Rao, J. Mater. Chem. 14 (2004) 1257.
[75] J.B. Parise, Y. Ko, J. Rijssenbeek, D.M. Nellis, K. Tan, S. Koch, Chem. Commun. (1994) 527.
[76] J.R. Allan, G.H.W. Milburn, F. Richmond, A.S. Wilson, D.L. Gerrard, J. Birnie, Thermochim. Acta 170 (1990) 147.
[77] H. Langfelderová, D. Makánová, P. Geri, J. Therm. Anal. 37 (1991) 2335.
[78] T.G. Fawcett, E.E. Bernarducci, K. Krogh-Jespersen, H.J. Schugar, J. Am. Chem. Soc. 102 (1980) 2598.
[79] E. Bernarducci, W.F. Schwindinger, J.L. Hughey IV, K. Krogh-Jespersen, H.J. Schugar, J. Am. Chem. Soc. 103 (1981) 1686.
[80] M. Eddaoudi, H.L. Li, O.M. Yaghi, J. Am. Chem. Soc. 122 (2000) 1391.
[81] A.P. Nelson, O.K. Farha, K.L. Mulfort, J.T. Hupp, J. Am. Chem. Soc. 131 (2009) 458.
[82] N. Jiang, A.J. Ragauskas, J. Org. Chem. 71 (2006) 7087.
[83] S. Mannam, S.K. Alamsetti, G. Sekar, Adv. Synth. Catal. 349 (2007) 2253.